Ionic transport in ABO_3 perovskite oxides: a computer modelling tour

M. Saiful Islam

Department of Chemistry, University of Surrey, Guildford, UK GU2 5XH.
E-mail: m.islam@surrey.ac.uk

This article presents a survey of recent applications of advanced computer modelling techniques in the study of ion transport and defect properties of ABO_3 perovskite-structured oxides. The principal methodologies are outlined which include techniques based upon both interatomic potentials (static lattice, molecular dynamics) and quantum mechanical methods. The scope of contemporary applications of computer modelling of perovskite oxides (such as $LaBO_3$ and $AZrO_3$) is illustrated by accounts of recent work on oxygen ion transport and defect association, on cation migration, and, finally, on proton incorporation and diffusion.

1 Introduction

Oxide materials that exhibit high ionic conductivity have attracted considerable attention for many years owing to both the range of applications (such as fuel cells, gas sensors, batteries, catalysts) and the fundamental fascination of ionic transport in crystalline solids.[1–9] The exploitation of ion fluxes through ionic or mixed conducting oxides now appears to be offering real technological opportunities; this includes oxide electrodes for solid oxide fuel cells (SOFCs)[1,10] and ceramic membranes designed to generate oxygen by separation from air.[1–3] Detailed overviews of the field can be obtained from several reviews.[1–10] It has become increasingly clear that the investigation of diffusion mechanisms and defect phenomena underpins both the understanding of macroscopic transport behaviour and the ability to predict transport parameters in solid materials. However, the majority of diffusion or conductivity experiments have difficulties in extracting enough information to identify the atomistic mechanisms (or local defect structures) controlling ionic transport.

It is now widely recognised that computer modelling techniques are well established tools in the field of materials chemistry, and have been applied successfully to studies of structures, energetics and dynamics of solids at the atomic level.[11,12] A major theme of modelling work has been the strong interaction with experimental studies, which is evolving in the direction of increasingly complex systems. The development of the field has also been assisted by the enormous growth in computer hardware power and by advances in theoretical methodologies. This review addresses recent trends and progress in the use of such computational techniques in the investigation of ionic transport in topical oxide materials.

One such family of oxides that has attracted considerable attention is based upon the perovskite structure of general formula ABO_3. This structure has been dubbed an "inorganic chameleon" as it displays a rich diversity of chemical compositions and properties. For example, the mixed ionic–electronic conductor $La_{1-x}Sr_xMnO_3$ finds use as the cathode material in solid oxide fuel cells,[1,10] whereas doped $LaGaO_3$ shows superior oxygen ion conductivity than the conventional zirconia-based electrolyte at moderate temperatures.[13] A range

of perovskite-structured ceramics, particularly cerates and zirconates,[14,15] exhibit high proton conductivity with potential "clean" applications in hydrogen fuel cell and sensor technologies. The fascinating and widely studied high T_c cuprate superconductors are also perovskite-based. More recently, the discovery of "colossal" magnetoresistance (CMR) in the manganates $Ln_{1-x}A_xMnO_3$ (where Ln = rare earth, A = Ca or Sr)[16] has stimulated further widespread interest. The majority of these perovskite oxides are acceptor doped with low-valent cations, giving rise to the formation of extrinsic oxygen vacancies and/or electronic species as charge-compensating defects; in the case of proton conduction, the oxygen vacancies are filled by hydroxy groups in the presence of water vapour.

In this article, I highlight contemporary computational work on different oxygen ion and proton-conducting perovskites (such as $LaBO_3$ and $AZrO_3$) to illustrate the breadth of information that can be obtained. Cation migration is also considered, a topic that has been paid limited attention. Emphasis is placed on probing the energetics and mechanisms of ionic transport (and associated defect properties), which have assisted in the further understanding of these complex oxides. Indeed, the principal aims of computer modelling have been to guide, interpret and stimulate experimental work (be it diffraction, spectroscopy or conductivity), and to have a predictive role in the design and improvement of materials. The review focuses on bulk transport properties, as up to now simulations have played a minor role in the study of surface diffusion in oxides. However, it is an area in which significant progress can be expected in the near future. First, this work is prefaced by a summary of the main computational techniques used in current studies.

2 Computational methods

The present account of these widely used techniques will be brief since comprehensive reviews are given elsewhere.[11,12,17,18]

The main simulation techniques used are, first, atomistic (static lattice) methods which determine the lowest energy configuration of the crystal structure by employing efficient energy minimisation procedures. The simulations rest upon the specification of an interatomic potential model which expresses the total energy of the system as a function of the nuclear coordinates. For ceramic oxides, the Born model framework is commonly employed which partitions the total energy into long-range Coulombic interactions, and the following short-range term to model the repulsions and van der Waals attractions between electron charge clouds:

$$\varphi_{ij}(r) = A_{ij} \exp(-r/\rho_{ij}) - (C_{ij}/r^6) \qquad (1)$$

Since charge defects will polarise other ions in the lattice, ionic polarisability must be incorporated into the potential model. The shell model[19] provides a simple description of such effects and has proven to be effective in simulating the dielectric and

DOI: 10.1039/a908425h

J. Mater. Chem., 2000, **10**, 1027–1038 **1027**

lattice dynamical properties of ceramic oxides. It should be stressed, as argued previously,[11] that employing such a potential model does not necessarily mean that the electron distribution corresponds to a fully ionic system, and that the general validity of the model is assessed primarily by its ability to reproduce observed crystal properties. In practice, it is found that potential models based on formal charges work well even for some semi-covalent compounds such as silicates and zeolites.[20] More recently, increased use has been made of energy minimisation techniques in refining approximately known structures, which is of particular value in the study of complex microporous systems.[11]

An important feature of these calculations is the treatment of lattice relaxation about the point defect, cluster or migrating ion. The Mott–Littleton approach is to partition the crystal lattice into two regions so that ions in a spherical inner region surrounding the defect are relaxed explicitly. In contrast, the remainder of the crystal, where the defect forces are relatively weak, is treated by more approximate quasi-continuum methods. In this way local relaxation is effectively modelled and the crystal is not considered simply as a rigid lattice. These methods are embodied in the GULP simulation code.[21]

The ABO_3 perovskite structure is built upon a framework of corner-linked BO_6 octahedra with the A cation in a 12-coordinate site; the orthorhombic phase can be considered as due purely to tilts of these octahedra from the ideal cubic configuration (shown in Fig. 1). The potential parameters for the oxide systems in this review were derived by empirical
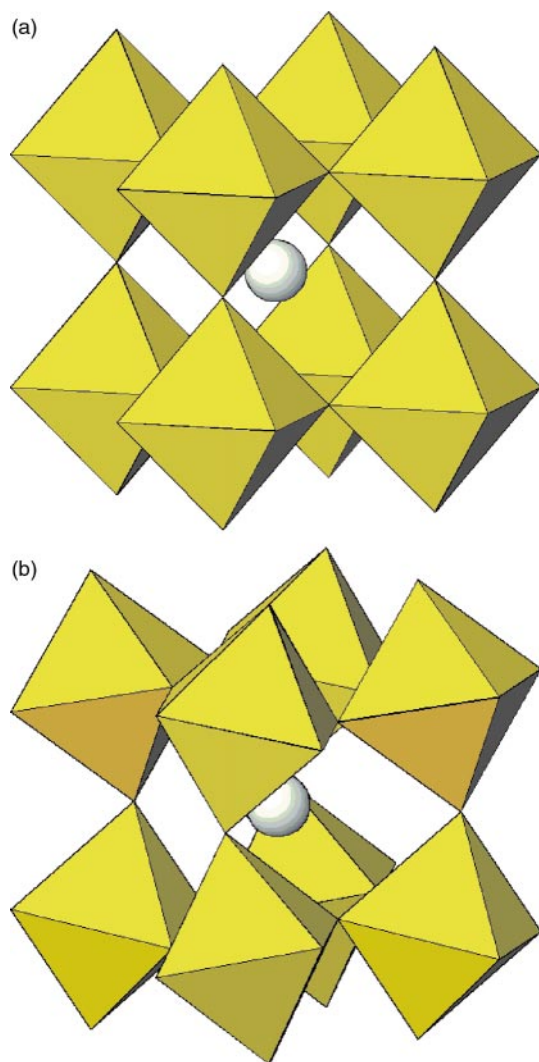

Fig. 1 Perovskite structure showing corner-linked BO_6 octahedra: (a) cubic, (b) orthorhombic.

procedures using their observed structures and crystal properties.[22,23] The calculated lattice parameters and their comparison with experimental values are listed in Table 1. Examination of the differences shows a good agreement between experimental and simulated structures. This provides a reliable starting point for the defect calculations.

A major thrust of fundamental transport studies has been the attempt to determine atomistic mechanisms controlling bulk transport behaviour. In the static lattice approach it is assumed that transport is effected by discrete jumps (or hops) of atoms by either vacancy or interstitial mechanisms. Given this hopping description, an adaptation of absolute rate theory[24] gives the following for the jump frequency:

$$v = v_0 \, \exp(-E_{act}/kT) \tag{2}$$

where the activation energy, E_{act}, is derived from simulating the potential energy surface for the migrating ion; this allows the identification of the maximum (or saddle-point) in the energy profile for the most favoured pathway. Such an approach has successfully been applied for over a decade in studies of defect transport in polar solids pioneered by Catlow.[11,12]

The second main type of simulation method is the molecular dynamics (MD) technique, which consists of an explicit dynamical simulation of the ensemble of particles for which Newton's equations of motion are solved numerically. Repetition of the integration algorithm yields a detailed picture of the evolution of ion positions and velocities as a function of time. This technique allows the inclusion of the kinetic energy for an ensemble of ions (to which periodic boundary conditions are applied) representing the system simulated. The system temperature is evaluated by calculating the average kinetic energy per particle:

$$T = 1/3Nk \langle \sum_{i=1}^{N} m_i v_i^2 \rangle \tag{3}$$

where N, m_i and v_i represent respectively the total number of particles, their masses and instantaneous velocities.[25] A time-step, Δt, is specified (typically 10^{-15} s) which is smaller than the time of any key dynamical process in the system, for example the period of atomic vibrations. The analysis of ion positions and velocities from the MD simulations generates a wealth of dynamical detail. Atomic transport properties are extracted using the time-dependent mean square displacements (MSD), defined as follows:

$$\langle r_i^2(t) \rangle = \frac{1}{N} \sum_{i=1}^{N} [r_i(t) - r_i(0)]^2 \tag{4}$$

where N is the total number of ions in the system. Mechanistic information can be obtained by analysis of particle trajectories. This includes highly correlated mechanisms in which ion transport is effected by several ions moving together in a concerted manner. In this way, point defects in the system (e.g. oxygen vacancies in a doped perovskite) can now be 'observed' to migrate between equilibrium sites, thus revealing the mechanism directly. However, the MD timescale is such that it is only practical to study fast diffusion processes. For example, MD methods (embodied in the DLPOLY code[26]) have been applied previously to superionic conductors, such as Na β''-Al_2O_3[27] and Y/ZrO_2[28] and to molecular diffusion in zeolites.[20,29]

Finally, there is an expanding role for quantum mechanical (QM) or first-principles methods in solid state studies, although they have not been applied widely to ionic transport in oxides. In general, such techniques attempt, at some level of approximation, to solve the Schrödinger equation for the system. They are thus able to provide detailed information on the electron density distribution. Hartree–Fock (HF) *ab initio* methods have been used in which all integrals (above a

Table 1 Calculated and experimental unit cell parameters of ABO_3 perovskite oxides

Compound	Unit cell symmetry	Lattice parameter	Calc./Å	Expt./Å[a]
LaMnO$_3$	Cubic	a	3.904	3.904
LaMnO$_3$	Orthorhombic	a	5.528	5.582
		b	5.553	5.583
		c	7.818	7.890
LaCoO$_3$	Cubic	a	3.820	3.823
LaGaO$_3$	Cubic	a	3.875	3.875
LaGaO$_3$	Orthorhombic	a	5.485	5.527
		b	5.481	5.496
		c	7.752	7.781
LaYO$_3$	Orthorhombic	a	6.052	6.086
		b	5.936	5.890
		c	8.512	8.511
BaCeO$_3$	Cubic	a	4.418	4.445
	Orthorhombic	a	8.816	8.791
		b	6.231	6.252
		c	6.243	6.227
CaZrO$_3$	Cubic	a	4.011	4.020
SrZrO$_3$	Cubic	a	4.095	4.101

[a]Experimental values from refs. 22, 23, 74.

threshold) are evaluated analytically or numerically.[18] Periodic HF methods (implemented in the CRYSTAL[30] package) have been used to study the electronic structure of transition metal oxides.[31] In addition, there has been recent progress in the study of defects in solids using "embedded" cluster techniques (using programs such as CADPAC[32]) in which the QM cluster is surrounded by some point charge representation of the rest of the crystal.[33] Techniques based on density functional theory (DFT) are now increasingly viewed as an important approach in materials science.[12,34] The essence of the local density approximation (LDA) to DFT is the use, in evaluating the total energy of the system, of expressions for the exchange and correlation energy that are appropriate to the homogeneous electron gas; contemporary work also emphasises the use of the generalised-gradient approximation (GGA). A widely used implementation of DFT combines a plane-wave basis set with the "pseudopotential" method, in which the pseudopotential represents the interaction between valence electrons and the atomic cores. This approach is also extended to first-principles dynamics (also called quantum molecular dynamics), which essentially combines the solution of the electronic structure with MD for the atoms (incorporated in the CASTEP package[35]). Illustrations of the application of QM or first-principles methods to proton migration will be given later in this paper. In general, QM studies serve to confirm the validity of the defect simulations, but provide additional information on the electronic structure that is inaccessible to atomistic simulations. The latter of course have the advantage of being computationally cheaper by several orders of magnitude.[11]

In an attempt to illustrate the energetic and mechanistic information that can be obtained by computational methods, the following sections highlight recent studies of ionic transport (oxygen ion, cation and proton) in perovskite-based oxides. Each area will demonstrate different types of transport behaviour that can be probed by modelling techniques.

3 Oxygen ion transport in LaBO$_3$

3.1 Migration pathway and energetics

The series of compounds based on LaBO$_3$ are some of the most fascinating members of the perovskite family, due to their applications in SOFCs, ceramic membranes and heterogeneous catalysis. The importance of understanding their transport behaviour has resulted in numerous studies of conductivity in systems mainly based upon doped LaCoO$_3$,[36–40] LaMnO$_3$[40–45] and LaGaO$_3$;[13,46–52] the latter material has attracted growing attention as a solid electrolyte competitive with Y/ZrO$_2$ (and

Gd/CeO$_2$) due to its extremely high oxygen ion conductivity at lower operating temperatures. A variety of techniques have been employed including ac/dc conductivity, secondary ion mass spectrometry (SIMS), thermogravimetric analysis and potentiostatic step methods. Overviews of the field of oxygen ion conductors can be obtained from recent reviews.[1,2,6]

Despite these various studies, the amount of information on fundamental mechanistic and defect processes has rather been limited. Atomistic simulation studies of Cherry[22] and Khan[23] et al. have been able to investigate these problems by an extensive search of the potential energy surface for oxygen vacancy migration. The energy profiles were mapped out by calculating the defect energy of the migrating ion along the diffusion path, and allowing relaxation of the lattice at each position. In this way the saddle-point configuration may be identified from which the energy barrier to migration is derived.

Interstitial formation and migration are calculated to be highly unfavourable as expected for the close-packed perovskite lattice. The simulations therefore confirm the migration of oxygen ion vacancies as the lowest energy path, as well as predicting that any oxygen hyperstoichiometry will not involve interstitial defects. The calculated migration energies accord well with the available experimental activation energies (Table 2), although direct comparison may not be straightforward since the observed values show significant variation. This scatter may reflect differences in experimental conditions, doping levels and oxygen stoichiometry, as well as problems with phase purity. Nevertheless, it is found that the calculated migration energy (0.73 eV) for the LaGaO$_3$ system is in good accord with activation energies of 0.66 and 0.727 eV from high temperature dc conductivity[47,50] and 0.79 eV from SIMS data.[48] It is observed that doped LaMnO$_3$ shows poor oxygen ion diffusivity in comparison to both LaCoO$_3$ and LaGaO$_3$ materials, which is attributed to the very low oxygen vacancy concentration.[40] It is important note that the

Table 2 Calculated and experimental energies for oxygen vacancy migration in LaBO$_3$ perovskites

Compound	E_m/eV[a]	
	Calc.	Expt.[b]
LaGaO$_3$	0.73	0.79, 0.66, 0.727
LaMnO$_3$	0.86	0.73
LaCoO$_3$	0.61	0.58, 0.78
LaYO$_3$	1.22	1.3

[a]1 eV = 96.486 kJ mol^{-1}. [b]Experimental values from refs. 36,37,42, 46–48.

calculated energies in Table 2 relate to intrinsic migration of oxygen vacancies and do not include energies of defect formation or association. These additional energy terms may account for the larger activation energies (>1 eV) that are found for certain dopant levels or for low temperature ionic conductivity,[40,49] a point discussed below.

It has been commonly assumed that the migrating ion within the perovskite lattice takes a direct linear path along the $\langle 110 \rangle$ edge of the BO_6 octahedron into a neighbouring vacancy. However, an important result of the search of the potential energy surface is that a small deviation from the direct path for vacancy migration is revealed; this is illustrated schematically in Fig. 2 and as a contour map in Fig. 3, the latter clearly showing the migration "channel". The calculations therefore reveal a curved route with the saddle-point away from the adjacent B site cation resulting in a significantly lower energy barrier.

In the saddle-point configuration the migrating ion must pass through the opening of a triangle defined by two A site (La^{3+}) ions and one B site ion. The simulation approach is able to model lattice relaxation and generate valuable information on local ion movements. It is worth recalling that ionic polarisability has been treated in the simulations by the shell model. Therefore, the perovskite structure is not considered simply as a hard-sphere lattice with fixed ions. From our analysis we find significant displacements (≈ 0.1 Å) of these cations away from the mobile oxygen ion. These results emphasise that neglecting lattice relaxation effects at the saddle-point may be a serious flaw in previous ion size approaches based on a rigid hard-sphere model, in which the 'critical radius' of the opening is derived. Indeed, our earlier work on ABO_3 showed a strong relationship between the perovskite tolerance factor (t) and the migration energy, in which the minimum seems to correspond to the most effective balance of the relaxation of A and B cations.[22]

Other notable examples of similar modelling work on related materials include studies of the high T_c superconductors[53] (e.g. $YBa_2Cu_3O_{7-x}$, $HgBa_2Ca_2Cu_3O_{8+\delta}$), the $A_2B_2O_5$ brownmillerite oxides, often viewed as oxygen-deficient perovskites (e.g. $Ba_2In_2O_5$[54]), and the Aurivillius family of oxygen ion conductors based upon a layered bismuth oxide/perovskite structure (e.g. BIMEVOX, Bi_2WO_6[55]). It should be stressed that a detailed survey of these systems is beyond the scope of this article, which focuses on perovskites of the ABO_3 type.

3.2 MD simulations of oxygen diffusion

An important factor for optimising the oxygen flux through oxides for electrochemical use is the rate of oxygen ion diffusion. Molecular dynamics techniques, in which kinetic energy terms are included explicitly, are well suited to probing the dynamical properties of solids, thus amplifying the information derived from static simulations. As noted in section 2, these techniques have been used to investigate a
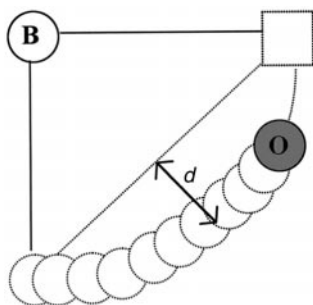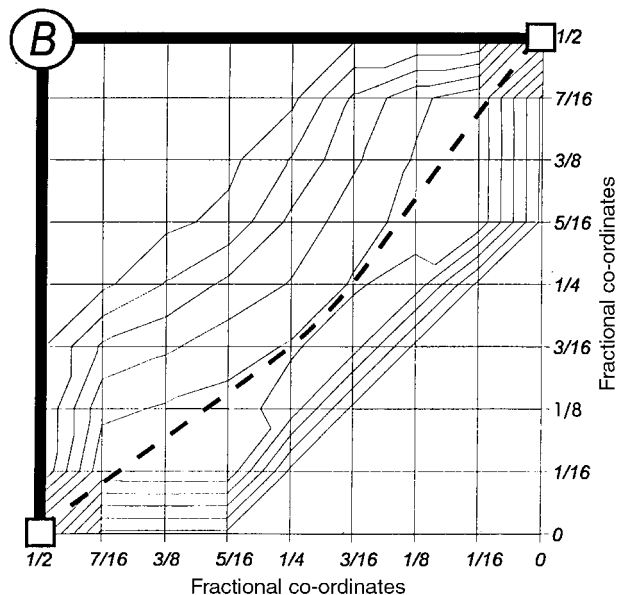
Fig. 3 Contour plot of potential energy surface for oxygen vacancy migration (showing the curved path or channel between adjacent anion sites).

variety of solid state ionics, although they have not widely been applied to ion diffusion in perovskite-type oxides.

Until recently,[26] the majority of MD studies have excluded the shell model treatment of ionic polarisation due to computational expense. Our recent studies have applied, for the first time, shell model MD to $LaCoO_3$ and $LaGaO_3$ based materials. Atomic transport parameters were extracted from the simulations using the time-dependent mean square displacements. Detailed analysis shows that only the oxygen ion MSDs increase with time indicating significant anion diffusion. Moreover, the mean square displacements allow contact with experiment via the diffusion coefficient (D_i) which can be obtained from the Einstein relation:

$$\langle r^2(t) \rangle = 6D_i t + B_i \tag{5}$$

The calculated oxygen diffusion coefficients for the gallate system have been derived in this way. We obtained a D value of 4.12×10^{-7} cm^2 s^{-1} at 1073 K for $La_{0.9}Sr_{0.1}Ga_{0.8}Mg_{0.2}O_{3-\delta}$ (LSGM) indicating that bulk oxygen diffusion is rapid; this is in good agreement with the only available observed value of 3.24×10^{-7} cm^2 s^{-1} from measurements using ^{18}O isotopic exchange and SIMS.[48] These experiments also indicate that the electrical conductivity is purely ionic, with no evidence of hole conduction. For the $La_{0.8}Sr_{0.2}CoO_{3-x}$ system we calculate diffusion coefficients of the order of 10^{-8} cm^2 s^{-1} in the same temperature region. In general, it is found that the oxygen diffusivity in doped $LaGaO_3$ is about an order of magnitude higher than in doped $LaCoO_3$.

Our main interest has been, however, in the mechanistic information revealed by the simulations. Analysis of the raw data of particle coordinates has enabled us to visualise the motion and dynamics by means of pictures of the ion trajectories. Fig. 4 clearly indicates small vibrations of the cations about their regular lattice sites in doped $LaGaO_3$, which is typical behaviour for an ordered, crystalline solid. In contrast, Fig. 5 shows a more diffuse distribution on the oxygen sublattice indicating significant ion motion: the diffusion of oxygen occurs by discrete hops between adjacent lattice sites along the GaO_6 octahedron edge in accord with our earlier atomistic static simulations. Furthermore, we find no evidence of correlated or concerted motion, but rather our simulations point to a conventional hopping mechanism.

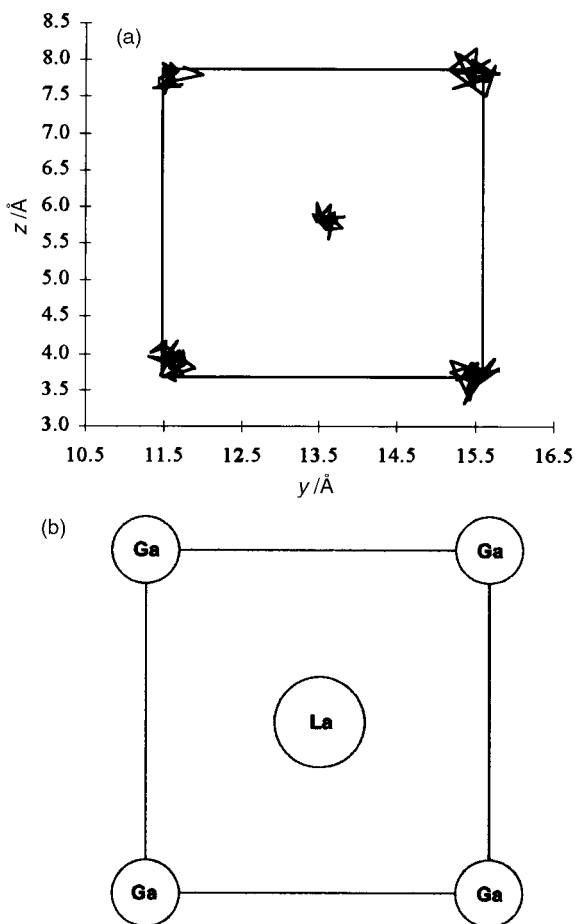Additional structural information was obtained from the

Fig. 2 Curved path for oxygen vacancy migration between adjacent anion sites.

Fig. 4 (a) Trajectory plots of host cations in doped $LaGaO_3$. (b) Schematic of ion positions in the unit cell.

pair radial distribution function (RDF), which provides an insight into the long-range (dis)order of the crystal lattice. The cation–cation RDFs (shown in Figs. 6 and 7) reveal a series of sharp peaks with the first five coordination shells clearly resolved in agreement with the observed ordered structure of $LaGaO_3$. In contrast, the oxygen–oxygen RDF (Fig. 8) show weak, diffuse structure for separations greater than nearest neighbour, indicative of greater disorder on the oxygen sublattice. This is particularly pronounced in the doped system showing lower maxima.

These perovskite materials therefore pose interesting structural features, that of a degree of disorder on one sublattice. Indeed, their features are similar to that found for fast-ion conductors ("superionics") in which the RDFs of the mobile sublattice are commonly more "melt-like" than those of normal crystalline solids.

3.3 Dopant substitution and defect clustering

The addition of aliovalent dopants is crucial to the ionic (or mixed) conductivity in $LaBO_3$ perovskites. These materials are typically acceptor-doped with divalent ions at the La^{3+} site, resulting in extrinsic oxygen vacancies at low vapour pressures. Considering Sr^{2+} substitution of La^{3+} as an example, this doping process can be represented by the following defect reaction:

$$SrO + La_{La}^x + \frac{1}{2}O_O^x = Sr'_{La} + \frac{1}{2}V_O^{\cdot\cdot} + \frac{1}{2}La_2O_3 \qquad (6)$$
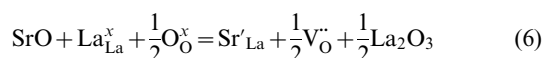
where, in Kroger–Vink notation, Sr'_{La} signifies a dopant substitutional and $V_O^{\cdot\cdot}$ an oxygen vacancy. Atomistic simulations have been used to evaluate the energies of this "solution" reaction by combining appropriate defect and lattice energy
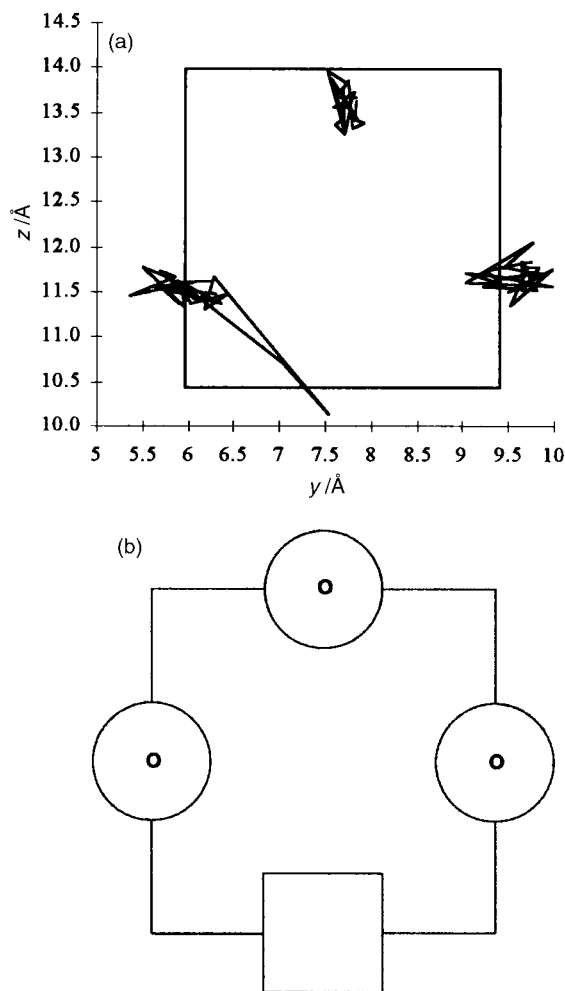

Fig. 5 (a) Trajectory plots of oxygen ions in doped $LaGaO_3$. (b) Schematic of ion positions in the unit cell with an oxygen vacancy.
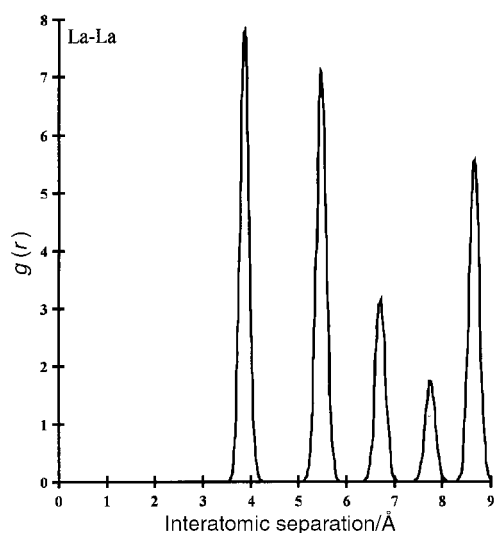

Fig. 6 Radial distribution functions for La ions in doped $LaGaO_3$.

terms. In this way, the modelling approach provides a useful systematic guide to the relative energies for different dopant species at the same site.

Detailed studies have calculated solution energies for a series of alkaline-earth metal ions in the $LaBO_3$ materials (B = Mn, Co or Ga).[22,23] The results, presented in Fig. 9, reveal that the lowest values are predicted for Sr and Ca at the La site. The favourable incorporation of these ions will therefore enhance
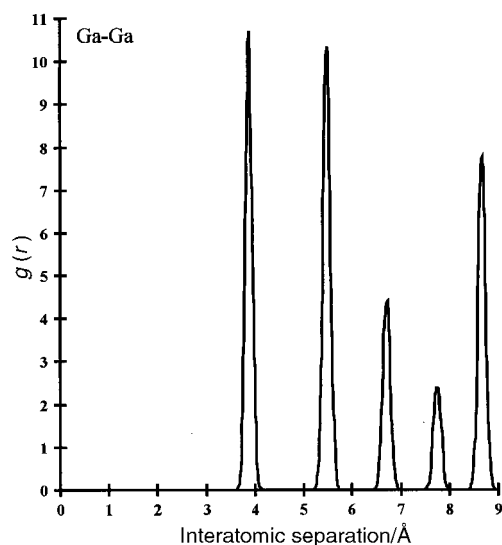
Fig. 7 Radial distribution functions for Ga ions in doped LaGaO₃.

Fig. 8 Radial distribution functions for oxygen ions in LaGaO₃: undoped (full line) and doped (dotted line).

transport properties owing to the increase in the concentration of mobile defects. These results accord well with experimental work in which Sr is the dopant commonly used to generate ionic (or mixed) conductivity in these perovskites, while Ca is often used to generate mixed valent Mn^{3+}/Mn^{4+} in the magnetoresistive (CMR) manganates. It is also apparent from Fig. 9 that a degree of correlation is found between the calculated solution energy and the size of the alkaline-earth dopant with minima near the radius of the host La^{3+}. However, ion size is not the sole factor as previous studies show that the solution energy for the alkali metal dopants of similar ionic radii are appreciably endothermic,[22,23] in line with their observed low solubility.

This approach has also been used as a predictive tool by extending the simulations to a wider range of dopant ions. Taking LaGaO₃ as an example, preliminary calculations find that Co, Cu, Ni have favourable solution energies on the Ga site. This predicts that these transition metal ions are promising candidates for use as acceptor dopants in LaGaO₃; any resulting mixed ionic–electronic conductivity is also of possible use in electrodes or separation membranes. Indeed, recent studies have shown mixed conductivity in Ni and Co doped LaGaO₃.[50] It is worth mentioning that in addition to ionic defects these modelling techniques have been used to investigate redox processes and the formation of electron/hole species in transition metal oxides[23,56] including the perovskite-based high T_c superconductors.[53]

It is well known that interactions between dopant ions and their charge-compensating defects can lead to the formation of distinct clusters which can "trap" the migrating species. For example, the oxygen ion conductivity of fluorite-structured oxides (such as Y-doped CeO₂) is largely controlled by the extent of dopant–vacancy interactions.[5] These have been described in terms of the formation of dopant–oxygen vacancy pair clusters with either the NN or NNN configuration, which add a binding (association) energy term to the conduction activation energy.[5,9]

In this context, recent conductivity measurements of $La_{1-x}Sr_xGa_{1-y}Mg_yO_{3-\delta}$ find significant differences in the activation energy as a function of Sr and Mg content.[46,49] Huang et al.[49] have noted the importance of the possible trapping of an oxygen vacancy at a divalent-cation impurity. However, the experimental determination of the detailed microstructures of defect clusters can be difficult. Consequently, Khan et al.[23] undertook a series of calculations on defect pair clusters in the LaGaO₃ system comprised of a
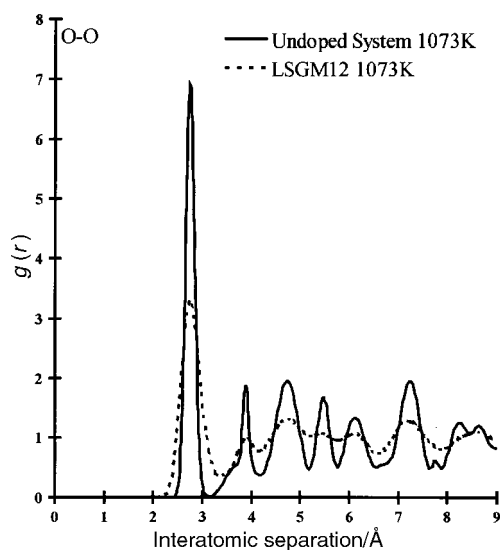
dopant substitutional and an oxygen vacancy at nearest-neighbour sites.

For both LaGaO₃ and LaCoO₃, the calculated cluster binding energies (E_b) with respect to the component isolated defects (Table 3) reveal that all the pair clusters are bound; the lowest E_b is for the Sr-vacancy configuration. In particular, a near-zero value is predicted for the Sr-vacancy ($Sr'_{La} V_O^{..}$) pair in LaGaO₃ although it is possible that other types of aggregate could have greater stability. This negligible binding term for the Sr dopant may be a major factor in promoting the observed high oxygen ion conductivity in the gallate perovskite. By contrast, Ca- or Mg-vacancy clusters are found to have higher binding energies in both LaGaO₃ and LaCoO₃ which points to greater trapping of the migrating oxygen vacancies. These results are consistent with the observed increase in the conduction activation energy at higher Mg doping levels (and at reduced temperatures) in $La_{1-x}Sr_xGa_{1-y}Mg_yO_{3-\delta}$.[46,49] This would lead to two distinct regions in the conductivity

Table 3 Calculated binding energies for {dopant–oxygen vacancy} pair clusters

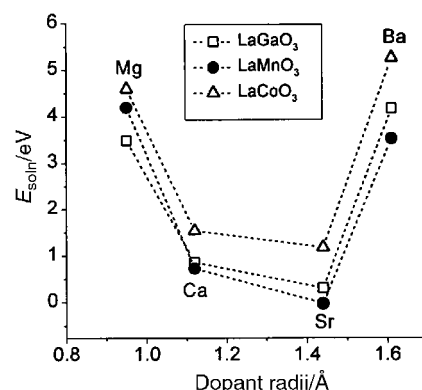| Compound	Dopant–vacancy pair	E_b/eV
LaGaO₃	$(Sr'_{La}V_O^{..})$	−0.02
	$(Ca'_{La}V_O^{..})$	−0.19
	$(Mg'_{Ga}V_O^{..})$	−1.37
LaCoO₃	$(Sr'_{La}V_O^{..})$	−0.19
	$(Ca'_{La}V_O^{..})$	−0.30
	$(Mg'_{Co}V_O^{..})$	−0.94

Fig. 9 Calculated energies of solution as a function of dopant ion radius for alkaline-earth cations substituting on the La site.

Arrhenius plot as found by Huang *et al.*[49] The high temperature region relates to purely the oxygen migration energy (E_m), whereas the low temperature region relates to E_m plus a binding (association) energy term.

Previous work on dopants in fluorite oxides has indicated that the elastic strain field around the defects in the cluster is at least as important as the electrostatic interaction.[5,11] The binding energy is therefore dependent upon the ion size 'mismatch' between the host and dopant cation with the expectation of a minimum when the ionic radii are approximately the same. This is borne out here with the greater ion size mismatch for the Mg^{2+} (0.72 Å) on the small Ga^{3+} site (0.62 Å).

Perhaps the most significant conclusion from the dopant calculations is that incorporation of Sr into $LaGaO_3$ will optimise the oxygen diffusivity owing to both the low binding energy term and the increase in vacancy concentration.

4 Cation transport

Despite numerous studies devoted to oxygen transport, little attention has been paid to cation diffusion in perovskite oxides, notwithstanding its significance to the reliability of technological applications. Cation migration plays an important role in the fabrication and processing of oxide ceramics, and also in the reverse process of degradation. The long term behaviour of devices incorporating such materials may depend on them maintaining their structure under mechanical load (creep) and their chemical composition under electrochemical potential gradients (kinetic demixing, interdiffusion). For ceramic membranes, it is believed that if the cation mobilities are different and non-negligible at high temperatures, concentration gradients appear in the oxide in such a way that the high oxygen pressure side tends to be enriched with the faster moving cation species.[3]

It is well known that $LaMnO_{3+\delta}$, is somewhat unusual in comparison to most other perovskite oxides in that it exhibits oxidative non-stoichiometry. Neutron powder diffraction[57–60] and simulation studies[61] have all indicated that cation vacancies, rather than oxygen interstitials, are responsible for the oxygen hyperstoichiometry. To date there have been no reports concerned with the direct determination of cation diffusion coefficients in the $LaMnO_3$ system. This is of particular importance in relation to their use as cathodes in SOFCs and as CMR materials. In an attempt to shed light on this problem De Souza *et al.*[61] have undertaken atomistic simulations of cation vacancy migration in cubic, orthorhombic and rhombohedral $LaMnO_3$.

It is apparent that lanthanum diffusion is most likely to take place by vacancy migration between neighbouring sites (in the $\langle 100 \rangle_{cubic}$ directions). The calculated activation energies for

Table 4 Calculated activation energies for cation vacancy migration in $LaMnO_3$
(a) La vacancy

Structure	E_m/eV	d_{O-O}/Å
Cubic	3.93	3.904
Rhombohedral	4.14	3.481
Orthorhombic	4.22	3.469

(b) Mn vacancy

Structure	E_m/eV	
	$\langle 110 \rangle_{cubic}$ diagonal	$\langle 100 \rangle_{cubic}$ curved
Cubic	14.71	7.73
Rhombohedral	14.00	8.82
Orthorhombic	14.11	9.94

this La vacancy mechanism, E_m^{La} (listed in Tables 4 and 5) indicate a clear trend towards higher energies as the perovskite lattice becomes more distorted from the cubic structure; this is associated with B–O–B bending and $[BO_6]$ octahedra tilting. The four surrounding oxygen ions at the saddle-point will provide a severe steric hindrance to A site migration. Accordingly, the calculations reveal a correlation between the shortest oxygen–oxygen separation across the octahedral interstice, d_{O-O}^{oct}, and the activation energy for La migration, E_m^{La}. As expected, E_m^{La} increases as d_{O-O}^{oct} decreases, since the steric hindrance is greater. Although there are no cation diffusion data for $LaMnO_3$, the predicted values for the vacancy mechanism are consistent with an experimental activation energy of 4.98 eV for La diffusion in the SOFC interconnect material $LaCrO_3$[62] and a calculated value of 4.7 eV for $LaGaO_3$.[23]
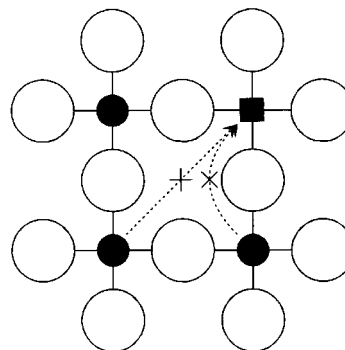

Fig. 10 Mn vacancy migration along diagonal and curved paths in $LaMnO_3$.

At first sight the obvious path for Mn migration in the perovskite lattice is between diagonal Mn sites in the $\langle 110 \rangle_{cubic}$ directions, as illustrated in Fig. 10. The calculated migration energies for this path are extremely high, lying around 14 eV for the three structures (Tables 4 and 5). However, lower activation energies were found for an alternative curved path between adjacent Mn sites along the $\langle 100 \rangle_{cubic}$ direction, for which the ion trajectory lies approximately in the $\{011\}_{cubic}$ plane. This is shown in Fig. 10 in which the migrating Mn cation moves up and around the oxygen ion. The much lower migration energies obtained for this curved path compared to those obtained for the diagonal path are attributed to a reduction in the repulsive La–Mn electrostatic interactions.

From creep experiments on $La_{1-x}Sr_xMnO_{3+\delta}$ samples, Wolfenstine *et al.*[63] extracted activation energies for bulk self diffusion, which varied between 4 and 5 eV, but they were unable to say whether these values referred to La, Sr or Mn self-diffusion. We have, therefore, modelled cation transport in Sr-doped and Ca-doped systems, in which the divalent dopant cations were compensated by electron holes (Mn^{4+} ions).

The results for A-site vacancy migration in the Sr- and Ca-doped compositions are shown in Fig. 11. For a particular dopant level the migration energies decrease in the order $E_m^{La} > E_m^{Sr} > E_m^{Ca}$, although the ionic radius of La^{3+} lies between that of Sr^{2+} and Ca^{2+}. This indicates that, as well as steric hindrance at the saddle point, electrostatic and ion polarisability factors are important. Our assertion of La diffusion being rate limiting agrees with the conclusions of van Roosmalen *et al.*[57] and of Stevenson *et al.*,[64] since we found that the activation energies for La migration increase with Mn^{4+} concentration. Moreover, our predicted energies for Ca vacancy migration (Fig. 11) are in good quantitative agreement with recent SIMS studies of Ca bulk diffusion in $La_{0.75}Ca_{0.25}CrO_3$ where activation energies of 2.1 to 2.5 eV were obtained under varying oxygen partial pressures.[65]
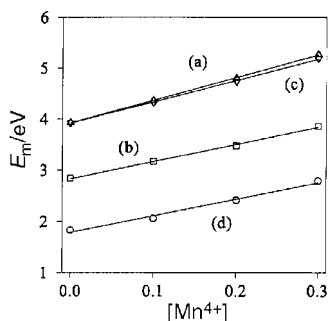
Fig. 11 Calculated activation energies for A-site migration in acceptor-doped cubic LaMnO$_3$: (a) E_m^{La} (La$_{1-x}$Sr$_x$MnO$_3$), (b) E_m^{Sr} (La$_{1-x}$Sr$_x$MnO$_3$), (c) E_m^{La} (La$_{1-x}$Ca$_x$MnO$_3$), (d) E_m^{Ca} (La$_{1-x}$Ca$_x$MnO$_3$).

5 Proton conductors

5.1 Water incorporation energetics

In addition to oxygen ion conduction, perovskite oxides have received considerable attention as high temperature proton conductors with promising applications in fuel cells, hydrogen sensors and steam electrolysers.[14,15] Most attention has focused on A^{2+}B^{4+}O$_3$ perovskites, particularly ACeO$_3$ (A = Sr or Ba)[66,67] and AZrO$_3$ (A = Ca or Sr).[68,69] There have only been a few studies on proton conductivity in A^{3+}B^{3+}O$_3$ type materials such as LaYO$_3$[70] and LaErO$_3$.[71] Recent developments have included the discovery of high proton conductivity in complex perovskites of the type A$_3$B'B''$_2$O$_9$ (*e.g.* Ba$_3$Ca$_{1.18}$Nb$_{1.82}$O$_9$ often termed BCN18), in which oxygen vacancies are created by varying the B' : B'' ratio.[15,72]

When these perovskite oxides are exposed to water vapour the oxygen vacancies are replaced by hydroxy groups in which the very small proton is not in a "free" state but closely associated with an oxygen ion. The water incorporation (or dissolution) reaction can be described as follows:

$$H_2O(g) + V_O^{\cdot\cdot} + O_O^x \rightarrow 2OH_O^{\cdot} \tag{7}$$
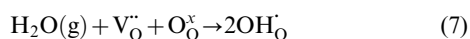
From the limited thermodynamic data available, it is found that the enthalpy for water incorporation, E_{H_2O}, is exothermic. This indicates that such materials will be dominated by protons at low temperatures and by oxygen vacancies at high temperatures. However, the magnitude of E_{H_2O} (sometimes termed the dissolution enthalpy[15]) varies with oxide system and determines the extent of protonation at a given temperature. It is clear that an understanding of the materials properties affecting the energetics of the incorporation reaction will enable a systematic selection of candidate proton conductors. In this context, computer modelling techniques are particularly valuable where other ionic or electronic defects may make it difficult to study protons at the microscopic level.

Recent computational work has investigated this problem by evaluating E_{H_2O} for a range of proton-conducting perovskites in which the O–H interaction is modelled as a Morse potential.[23,73,74] This energy was evaluated using the following equation:

$$E_{H_2O} = 2E_{OH} - E(V_O^{\cdot\cdot}) + E_{PT} \tag{8}$$

where E_{OH} is the energy associated with substitution by the hydroxy group, $E(V_O^{\cdot\cdot})$ the energy of an oxygen vacancy, and E_{PT} the energy of the gas phase proton transfer reaction: O^{2-} + H$_2$O → 2OH$^-$.

The calculated values of E_{H_2O} for a range of topical proton conductors, namely BaCeO$_3$, SrZrO$_3$, CaZrO$_3$ and LaYO$_3$, are listed in Table 6. It is predicted that water incorporation is exothermic for all four systems. This is in agreement with experiment where it is found that proton uptake in such perovskites increases with decreasing temperature. There are, of course, uncertainties in the absolute calculated values due to

the free-ion energies employed. Nevertheless, there is reasonable quantitative accord with the limited experimental values that are available. For example, thermal analysis measurements on doped BaCeO$_3$[75] yielded water incorporation enthalpies in the range −1.32 to −1.84 eV as a function of Y doping (2 to 20 mol%). Thermodynamic studies[15] of Yb-doped SrZrO$_3$ gave an exothermic value of −1.10 eV. Although there are no specific data on LaYO$_3$ for direct comparison, the predicted energy is consistent with the experimental value of −1.91 eV for the similar perovskite La$_{0.9}$Sr$_{0.1}$ErO$_{3-x}$.[71] In contrast to both LaYO$_3$ and LaErO$_3$, recent calculations on LaGaO$_3$ find a highly positive incorporation energy.[23] In agreement with this prediction, no evidence of proton transport has been found in acceptor-doped LaGaO$_3$ from total conductivity experiments as a function of water vapour pressure.[52]

It has been observed that for proton conductors the incorporation energy becomes increasingly negative with increasing levels of acceptor doping, as we find from our simulations (Table 6). Analysis of the calculated component terms to E_{H_2O} by Davies *et al.*[74] indicates that the most significant change with dopant content is the reduction in E_{OH} (associated with substitution of O^{2-} with OH$^-$) whereas the oxygen vacancy energy remains essentially constant.[74] The variation in E_{OH} may reflect a change in the strength of OH bonding and suggests an energetic stabilisation of the protonic defect with doping. This trend has also been related to the increased basicity of the oxide lattice.[75] It is worth noting here that similar calculations have been performed on proton insertion in the spinel-structured lithium manganates (λ-MnO$_2$–LiMn$_2$O$_4$),[76] which are important materials for advanced lithium batteries and as ion-selective sorbents.

Conflicting debate on proton-conducting perovskites has emerged as to whether there are any significant interactions between the protonic defect and the dopant ion, which may lead to association (or trapping). Kreuer *et al.*[75] suggest that the observed increase in activation energy for the diffusivity of protonic defects with increasing dopant content may be related to the general increase of the oxygen basicity and the proton-transfer barrier rather than proton-dopant association. In contrast, neutron vibrational spectroscopic studies of Karmonic *et al.*[77] suggest the presence of a considerable amount of protons associated with the dopant in doped SrCeO$_3$. Muon spin relaxation measurements on Sc-doped SrZrO$_3$[78] also suggest the existence of trapping centres adjacent to the dopant ion.
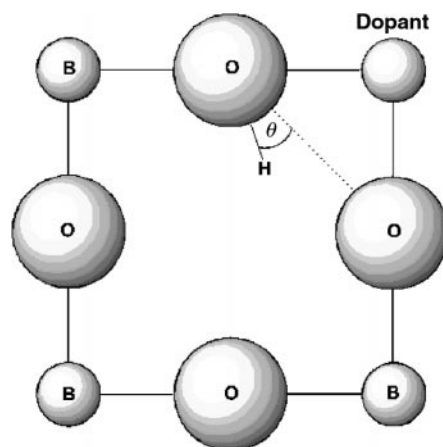

Fig. 12 Proton–dopant pair at nearest-neighbour sites in the [B–O] plane.

In an attempt to shed light on this problem, Davies *et al.*[74] have undertaken a series of calculations on defect pairs

Table 5 Calculated energies of water incorporation (E_{H_2O}) [based on reaction (7)]

| Dopant level (x) | E_{H_2O}/eV | | | |
	$BaCe_{1-x}Y_xO_3$	$CaZr_{1-x}Y_xO_3$	$SrZr_{1-x}Y_xO_3$	$La_{1-x}Sr_xYO_3$
0.05	−0.75	−1.22	−0.46	−0.65
0.10	−1.01	−2.21	−1.11	−1.36

comprised of an OH group and a dopant substitutional at nearest-neighbour sites (Fig. 12). Attention was focused on the most favourable dopants, Sc^{3+}, Yb^{3+} and Y^{3+}, in the $SrZrO_3$ system. Negative binding (association) energies were calculated in the range −0.4 to −0.7 eV, which predict that all the OH–dopant pairs are bound. The magnitude of the binding energy is different for the three dopants, with the relative order $Sc^{3+} > Y^{3+} > Yb^{3+}$. Such defect association may lead to an increase in the conduction activation energy with increasing dopant concentration. Indeed, the proton conductivity for Yb^{3+}-doped $SrZrO_3$ is higher than that found for the Sc-doped system. Our calculated binding energies are also consistent with the "trapping" energies derived from spectroscopic studies[77,78] which fall in the range −0.2 to −0.4 eV, although our values are slightly higher. In any case, the simulations predict that proton–dopant association may occur, which would be a major factor limiting the proton mobility at higher dopant levels. This picture can be viewed as analogous to how the oxygen ion conductivity of fluorite (and perovskite) oxides is affected by dopant–vacancy interactions.

5.2 Proton transport mechanism

Isotope effect (H^+/D^+) measurements of perovskite oxides[72] have suggested that the conduction mechanism is due to proton hopping between adjacent oxygen ions (Grotthuss-type mechanism), rather than by hydroxyl ion migration ("vehicle" mechanism). These studies also imply that the proton jump involves quantum effects (tunnelling) and that co-operative motions of the structure (lattice phonons) will lead to modulations of the O–O separations.

Further to understand the underlying transport mechanism, the proton transfer process has been investigated by Cherry and coworkers[73] using *ab initio* Hartree–Fock techniques (embodied in the CADPAC code[32] as discussed in section 2). An embedded cluster of 13 lattice ions was used with the surrounding crystal lattice represented by an array of point charges which reproduce the correct electrostatic potential. The calculations were based upon the $LaAlO_3$ system, with high quality basis sets: Al 8-511G, O 8-411G, and H 6-311G. The calculations were performed at the SCF HF level with single point correlation effects included by the addition of Møller–Plesset perturbation theory to the second order (MP2). In this work, the energy barrier to proton transfer by a simple hopping mechanism was evaluated as the difference in energy between two states: (i) the ground state in which the single hydrogen is effectively bound to an oxygen ion, and (ii) the barrier state in which the hydrogen is equidistant between both the adjacent oxygen ions (illustrated in Fig. 13). The calculated barrier energy as a function of O–O separation is presented in Table 6. The results reveal that all the energies are very small, the lowest of ≈ 0.02 eV is only of the order of the zero point energy of the free OH^- species, although the magnitude increases slightly with increasing O–O separation.

With regard to the ground state configuration, the predicted O–H geometry has the proton site near the direction of one neighbouring oxygen ion with an equilibrium O–H bond distance of 0.94 Å. The relaxed geometry of the barrier state configuration (illustrated in Fig. 13) shows the importance of the O–O separation in the transfer process, as discussed by Kreuer.[14] The initial (unrelaxed) and final (relaxed) O–O
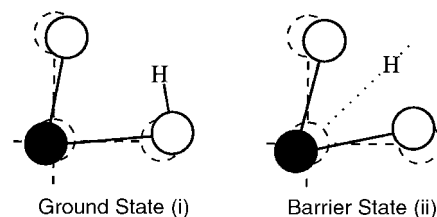
Fig. 13 Ground and barrier state configurations for proton transfer between neighbouring oxygen ions. (Dashed and full lines indicate perfect lattice and relaxed geometries respectively.)

Table 6 Energy barrier to proton transfer with initial and final O–O separation for the barrier state configuration

Initial O–O separation (unrelaxed)/Å	Final O–O separation (relaxed)/Å	Energy/ eV
2.67	2.32	0.02
2.76	2.35	0.04
2.90	2.38	0.16

separations from the barrier state calculations are also presented in Table 6; they clearly indicate that in each case the separation reduces to below 2.4 Å so as to assist proton transfer. This result corresponds to a significant hydrogen bond interaction, which contracts the O–O distance so the proton is not transferred through a totally "free" state. A Mulliken population analysis also indicates significant electronic interaction in the ground state configuration with the reduction of the effective charge (by −0.12 electron) of the adjacent oxygen ion to which the proton hops.[73] Quantum MD studies of cubic perovskites[79] find that the proton locally "softens" the lattice to allow the transient formation of hydrogen bonds and the proton transfer between neighbouring oxygen sites. These simulations have also suggested that proton transfer rather than hydroxyl ion reorientation (or rotation) is the rate-limiting step for proton conductivity.

Our calculated energy barriers of less than 0.2 eV are, however, well below the observed activation energies of the order 0.4 to 0.7 eV for proton conductivity in perovskite-type oxides.[66–72] Does this difference suggest that the activation energy for proton migration depends on other energy terms? For the proton transfer process our *ab initio* cluster calculations yield the energy and geometry of the ground and barrier state configurations. However, they provide no information concerning the relaxation of the surrounding lattice which would accompany the proton migration. Moreover, if protons migrate by a "barrier-less" jump or by a tunnelling process it will be essential that lattice relaxation achieves an equivalent environment around the two oxygen sites before transfer can occur. In other words, for proton tunnelling to occur it is known that states of identical energy should be available on both sides of the barrier. Migration would thus occur *via* the process shown schematically in Fig. 14.

Atomistic simulations have been performed to evaluate this "relaxation" energy (E_{relax}), *i.e.*, the energy required to move from the initial ground state with the proton bound to one oxygen ion to the intermediate state where the oxygen ions are in equivalent environments. It is significant that we find a value
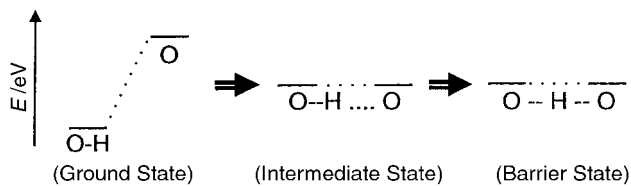
Fig. 14 Schematic representation of the proton transfer process indicating equilibration of the energy levels of the two adjacent oxygen ions.

of 0.69 eV for E_{relax} which correlates with observed activation energies for proton conductivity in perovskite oxides, and is consistent with measured activation energies of 0.7 eV for doped $LaYO_3$[16] and 0.42–0.50 eV for doped $LaErO_3$.[17] The calculations therefore suggest that a key step before proton transfer is the energy required for the neighbouring oxide ions to acquire equivalent lattice environments. This relaxation effect is predicted to favour structures with only one type of crystallographic oxygen site, as in cubic perovskites, which avoids extra terms associated with energy differences between non-equivalent positions.

This work has been extended recently to a preliminary first-principles dynamical study of proton diffusion in orthorhombic $CaZrO_3$, which involve computationally expensive simulations. As noted in section 2, recent developments have made the DFT-pseudopotential techniques powerful tools for accurate calculations of materials' properties.[12,34] Our first-principles dynamics simulations are based on optimised, norm-conserving pseudopotentials with electronic exchange correlation treated using the generalised gradient approximation (incorporated in the CASTEP code[35]). The initial optimisation reproduces the orthorhombic crystal structure to within 0.5% of the observed lattice parameters and cell volume. The dynamical simulations used a periodically repeated system of four $CaZrO_3$ unit cells and one H at a temperature of 1000 K. Full simulation details are given elsewhere.[80]

Primary interest here is in the information on the microscopic mechanism revealed by the calculations. Graphical analysis of the results shows a number of proton hopping events during the simulation run. Fig. 15 presents "snapshots" of one of these proton hops between neighbouring oxygen ions illustrating both ground and barrier (transition) states. This confirms that proton conduction occurs *via* a simple transfer of a proton from one oxygen ion to the next. As with previous QM studies,[79] we find rapid rotational motion of the proton in the O–H group, which allows the reorientation of the proton towards the next oxygen ion before the transfer process. The simulations also reveal predominantly inter-octahedra proton hopping rather than within octahedra. This appears to be influenced by the $[ZrO_6]$ tilting within the orthorhombic structure of $CaZrO_3$, which leads to close O–O separations between connecting octahedra for proton transfer (shown in Fig. 15). Furthermore, the dynamical simulations show considerable perturbation of the local lattice associated with proton motion; in addition to the reduction of the O–O
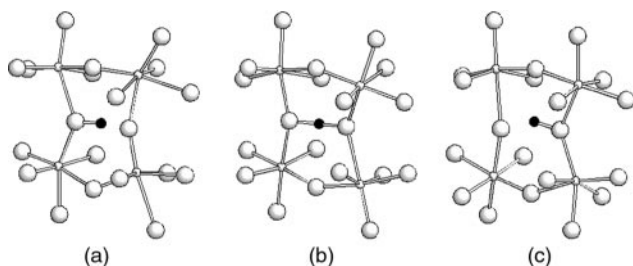
separation at the barrier state (to about 2.4 Å), we find displacements of up to 0.08 Å of other neighbouring oxygen ions suggesting the important role of hydrogen bonding to these oxygen ions. Further studies of these proton-conducting systems using first-principles methods are in progress.

6 Conclusion and future outlook

The survey presented in this article has aimed to demonstrate the valuable role that computational techniques now play in contemporary studies of perovskite-structured conductors. Such modelling tools, acting as powerful "computational microscopes", have been able to provide deeper fundamental insight as to the structures and dynamics of these complex oxides on the atomic scale. In particular, the simulations have unravelled unique mechanistic detail, and have made predictions on ion transport and defect association. The results on oxygen ion, proton and cation migration are compatible with the available experimental data. Moreover, the simulation studies have aimed to illuminate, guide and stimulate further work on these materials, relevant to their applications in "clean technology" such as solid oxide fuel cells, oxygen separation membranes and partial oxidation reactors.

Extension of the current modelling work on ABO_3 perovskites is expected on surface and interfacial phenomena, and on the growing use of *ab initio* dynamical methods to probe proton transport, as in, for example, new mixed proton–electron conductors, for which we have limited mechanistic knowledge. Future work also should explore the transport properties of related classes of oxides such as the Ln_2NiO_4-type materials (with the K_2NiF_4 structure), the brownmillerite-related $SrFeCo_{0.5}O_x$ and the complex perovskites $A_3B'B''_2O_9$ with the prototype composition $Ba_3CaNb_2O_9$.

In general, key developments in materials modelling are likely to encompass the greater use of shell model MD over longer timescales, and the extension of quantum mechanical or first-principles techniques to more complex systems, with increasing emphasis on predictive calculations. These developments will be assisted by the constant growth in computer resources, and will also draw on the strong interaction with complementary experimental techniques.

Fig. 15 Sequence of three snapshots from dynamical simulations showing inter-octahedra proton hopping in orthorhombic $CaZrO_3$. (The Ca ions are omitted for clarity.)

References

1 B. C. H. Steele, *Solid State Ionics*, 1996, **86–88**, 1223; *Curr. Opin. Solid State Mater. Sci.*, 1996, **1**, 684; J. A. Kilner, S. Benson, J. Lane and D. Waller, *Chem. Ind. (London)*, 1997, **22**, 911.
2 J. C. Boivin and G. Mairesse, *Chem. Mater.*, 1998, **10**, 2870.
3 H. J. M. Bouwmeester and A. J. Burgraff, in *Fundamentals of Inorganic Membrane Science and Technology*, eds. A. J. Burgraff and L. Cot, Elsevier, Amsterdam, 1996.
4 R. Doshi, J. L. Routbort and C. B. Alcock, *Def. Diff. Forum*, 1996, **127**, 39.
5 H. L. Tuller and M. Balkanski (Editors), *Science and technology of fast-ion conductors*, Plenum Press, New York, 1987; H. L. Tuller, *J. Phys. Chem. Solids*, 1994, **55**, 1393.
6 K. R. Kendall, C. Navas, J. K. Thomas and H. C. zur Loye, *Solid State Ionics*, 1995, **82**, 215.
7 P. J. Gellings and H. J. M. Bouwmeester, *Catal. Today*, 1992, **1**, 1.

8   P. G. Bruce (Editor), *Solid State Electrochemistry*, CUP, Cambridge, 1997; A. R. West, *J. Mater. Chem.*, 1991, **1**, 157.

9   G. E. Murch and A. S. Nowick (Editors), *Diffusion in crystalline solids*, Academic Press, New York, 1984.

10   N. Q. Minh, *J. Am. Ceram. Soc.*, 1993, **76**, 563.

11   C. R. A. Catlow, in *Solid State Chemistry: Techniques*, eds. A. K. Cheetham and P. Day, Clarendon Press, Oxford, 1987; C. R. A. Catlow (Editor), *Computer Modelling in Inorganic Crystallography*, Academic Press, San Diego, 1997.

12   *Faraday Discuss., R. Soc. Chem.*, 1997, 106.

13   T. Ishihara, H. Matsuda and Y. Takita, *J. Am. Chem. Soc.*, 1994, **116**, 3801.

14   K. D. Kreuer, *Chem. Mater.*, 1996, **8**, 610; *Solid State Ionics*, 1997, **94**, 55; H. Iwahara, *Solid State Ionics*, 1996, **86–88**, 915.

15   T. Norby and Y. Larring, *Curr. Opin. Solid State Mater. Sci.*, 1997, **2**, 593; T. Norby, *Solid State Ionics*, 1999, **125**, 1.

16   R. M. von Helmholt, J. Wecker, B. Holzapfel, L. Schultz and K. Samwer, *Phys. Rev. Lett.*, 1993, **71**, 2331; S. Jin, T. H. Tiefel, M. McCormack, R. A. Fastnacht, R. Ramesh and L. H. Chen, *Science*, 1994, **264**, 413; C. N. R. Rao and B. Raveau (Editors), *Colossal mangnetoresistance and related properties*, World Scientific, Singapore, 1998.

17   M. Meyer and V. Pontikis (Editors), *Computer simulation in materials science*, Kluwer, Dordrecht, 1991.

18   R. Dovesi, C. Pisani and C. Roetti, *Hartree–Fock ab initio treatment of crystalline systems*, Springer, Berlin, 1988, vol. 48.

19   B. G. Dick and A. W. Overhauser, *Phys. Rev.*, 1958, **112**, 90.

20   G. Sastre, C. R. A. Catlow and A. Corma, *J. Phys. Chem. B*, 1999, **103**, 5187; K. P. Schroder and J. Sauer, *J. Phys. Chem.*, 1996, **100**, 11043.

21   J. D. Gale, *J. Chem. Soc., Faraday Trans.*, 1997, 629.

22   M. Cherry, M. S. Islam and C. R. A. Catlow, *J. Solid State Chem.*, 1995, **118**, 125; G. V. Lewis and C. R. A. Catlow, *J. Phys. C*, 1985, **18**, 1149.

23   M. S. Khan, M. S. Islam and D. R. Bates, *J. Phys. Chem. B*, 1998, **102**, 3099.

24   G. Vineyard, *J. Phys. Chem. Solids*, 1957, **3**, 157.

25   V. Pontikis, *Phys. World*, 1990, 25.

26   W. Smith and T. R. Forester, *J. Mol. Graphics*, 1994, **14**, 136.

27   W. Smith and M. J. Gillan, *J. Phys.: Condens. Matter*, 1992, **4**, 3215.

28   M. S. Khan, M. S. Islam and D. R. Bates, *J. Mater. Chem.*, 1998, **8**, 2299; H. W. Brinkman, W. J. Briels and H. Verweij, *Chem. Phys. Lett.*, 1995, **247**, 386.

29   P. Demontis and G. B. Suffritti, *Chem. Rev.*, 1997, **97**, 2845; D. A. Faux, W. Smith and T. R. Forester, *J. Phys. Chem. B*, 1997, **101**, 1762.

30   R. Dovesi, V. R. Saunders, C. Roetti, M. Causa, N. M. Harrison, R. Orlando and E. Apra, CRYSTAL95, University of Torino, Italy, 1996.

31   N. M. Harrison, V. R. Saunders, R. Dovesi and W. C. Mackrodt, *Philos. Trans. R. Soc. London, Ser. A*, 1998, **356**, 75; F. Cora and C. R. A. Catlow, *Solid State Ionics*, 1998, **12**, 131.

32   R. D. Amos, CADPAC program, Cambridge University, 1992.

33   G. Pacchioni, A. M. Ferrari and G. Ierano, *Faraday Discuss. R. Soc. Chem.*, 1997, **106**, 155; J. L. Pascual and L. G. M. Pettersson, *Chem. Phys. Lett.*, 1997, **270**, 351.

34   R. Shah, J. D. Gale and M. C. Payne, *Chem. Commun.*, 1997, 131; P. J. D. Lindan, N. M. Harrison and M. J. Gillan, *Phys. Rev. Lett.*, 1998, **80**, 762; J. Bernholc, *Phys. Today*, 1999, **52**, 30.

35   M. C. Payne, M. P. Teter, D. C. Allan, T. A. Arias and J. D. Joannopoulos, *Rev. Mod. Phys.*, 1992, **64**, 1045.

36   T. Ishigaki, S. Yamauchi, K. Kishio, J. Mizusaki and K. Fueki, *J. Solid State Chem.*, 1988, **73**, 179; J. Mizusaki, *Solid State Ionics*, 1992, **52**, 79.

37   S. Carter, A. Selcuk, R. J. Chater, J. Kajda, J. A. Kilner and B. C. H. Steele, *Solid State Ionics*, 1992, **53–56**, 597.

38   V. V. Kharton, A. V. Kovalevsky, V. N. Tikhonovich, E. N. Naumovich and A. P. Viskup, *Solid State Ionics*, 1998, **110**, 53.

39   R. H. E. van Doorn, I. C. Fullarton, R. A. de Souza, J. A. Kilner, H. J. M. Bouwmeester and A. J. Burgraaf, *Solid State Ionics*, 1997, **96**, 1.

40   R. A. de Souza and J. A. Kilner, *Solid State Ionics*, 1998, **106**, 175.

41   J. Kjaer, I. G. Krogh Andersen and E. Skou, *Solid State Ionics*, 1998, **113–115**, 387.

42   A. Belzner, T. M. Gur and R. A. Huggins, *Solid State Ionics*, 1992, **57**, 327.

43   I. Yasuda and M. Hishinuma, *J. Solid State Chem.*, 1996, **123**, 382.

44   P. D. Petrolekas and I. S. Metcalfe, *J. Catal.*, 1995, **152**, 147.

45   A. V. Berenov, J. L. MacManus-Driscoll and J. A. Kilner, *Solid State Ionics*, 1999, **121**, 41.

46   P. Huang and A. Petric, *J. Electrochem. Soc.*, 1996, **143**, 1644.

47   J. Drennan, V. Zelizko, D. Hay, F. T. Ciacchi, S. Rajendran and S. P. Badwal, *J. Mater. Chem.*, 1997, **7**, 79.

48   T. Ishihara, J. A. Kilner, M. Honda and T. Takita, *J. Am. Chem Soc.*, 1997, **119**, 2747; T. Ishihara, T. Akbay, H. Furatani and Y. Takita, *Solid State Ionics*, 1998, **113–115**, 585.

49   K. Huang, R. S. Tichy and J. B. Goodenough, *J. Am. Ceram. Soc.*, 1998, **81**, 2565.

50   H. Ullmann and N. Trofimenko, *Solid State Ionics*, 1999, **119**, 1.

51   P. R. Slater, J. T. S. Irvine, T. Ishihara and T. Takita, *J. Solid State Chem.*, 1998, **139**, 135; N. M. Sammes, G. A. Tompsett, R. J. Phillips and A. M. Cartner, *Solid State Ionics*, 1998, **111**, 1; J. W. Stevenson, T. R. Armstromg, L. R. Pederson, J. Li, C. A. Lewinsohn and S. Baskaran, *Solid State Ionics*, 1998, **113–115**, 571.

52   M. Feng and J. B. Goodenough, *Eur. J. Solid State Inorg. Chem.*, 1994, **31**, 663.

53   M. S. Islam and L. J. Winch, *Phys. Rev. B*, 1995, **52**, 10510; M. S. Islam and R. C. Baetzold, *J. Mater. Chem.*, 1994, **4**, 299; N. L. Allan and W. C. Mackrodt, *Philos. Mag. A.*, 1991, **64**, 1129.

54   C. A. J. Fisher and M. S. Islam, *Solid State Ionics*, 1999, **118**, 355.

55   M. S. Islam, S. Lazure, R. N. Vannier, G. Nowogrocki and G. Mairesse, *J. Mater. Chem.*, 1998, **8**, 655; C. Piravano, M. S. Islam, R. N. Vannier, G. Nowogrocki and G. Mairesse, to be published.

56   H. Donnerberg and A. Birkholz, *J. Phys. Condens. Matter*, 1995, **7**, 327; R. W. Grimes, D. J. Binks and A. B. Lidiard, *Phil. Mag. A*, 1995, **72**, 651; S. C. Parker, E. T. Kelsey, P. M. Oliver and J. O. Titiloye, *Faraday Trans.*, 1993, **95**, 75.

57   J. A. M. van Roosmalen, E. H. P. Cordfunke, R. B. Helmholdt and H. W. Zandberg, *J. Solid State Chem.*, 1994, **110**, 100.

58   J. F. Mitchell, D. N. Argyriou, C. D. Potter, D. G. Hinks, J. D. Jorgensen and S. D. Bader, *Phys. Rev. B*, 1996, **54**, 6172.

59   J. A. Alonso, M. J. Martinez-Lope, M. T. Casais, J. L. MacManus-Driscoll, P. S. I. P. N. de Silva, L. F. Cohen and M. T. Fernandez-Diaz, *J. Mater. Chem.*, 1997, **7**, 2139.

60   Q. Huang, A. Santoro, J. W. Lynn, R. W. Erwin, J. A. Borchers, J. L. Peng and R. L. Greene, *Phys. Rev. B*, 1997, **55**, 14987.

61   R. A. De Souza, M. S. Islam and E. Ivers-Tiffe, *J. Mater. Chem.*, 1999, **9**, 1621.

62   T. Akashi, M. Nanko, T. Maruyama, Y. Shiraishi and J. Tanabe, *J. Electrochem. Soc.*, 1998, **145**, 2090.

63   J. Wolfenstine, K. C. Goretta, R. E. Cook and J. L. Routbort, *Solid State Ionics*, 1996, **92**, 75.

64   J. W. Stevenson, P. F. Hallman, T. R. Armstrong and L. A. Chick, *J. Am. Ceram. Soc.*, 1995, **78**, 507.

65   T. Horita, M. Ishikawa, K. Yamaji, N. Sakai, H. Yokokawa and M. Dokiya, *Solid State Ionics*, 1999, **124**, 301.

66   T. Yajima and H. Iwahara, *Solid State Ionics*, 1992, **50**, 281; J. F. Liu and A. S. Nowick, *Solid State Ionics*, 1992, **50**, 131; D. Shima and S. M. Haile, *Solid State Ionics*, 1997, **97**, 443.

67   N. Bonanos, K. S. Knight and B. Ellis, *Solid State Ionics*, 1995, **79**, 161; R. C. T. Slade, S. D. Flint and N. Singh, *J. Mater. Chem.*, 1995, **4**, 509; J. Guan, S. E. Morris, U. Balachandran and M. Liu, *Solid State Ionics*, 1998, **110**, 303.

68   J. A. Labrincha, J. R. Frade and F. M. B. Marques, *Solid State Ionics*, 1993, **61**, 71; L. Zimmermann, H. G. Bohn, W. Schilling and E. Syskakis, *Solid State Ionics*, 1995, **77**, 163.

69   T. Schober, J. Friedrich and J. B. Condon, *Solid State Ionics*, 1995, **77**, 175; H. Yugami, S. Matsuo and M. Ishigame, *Solid State Ionics*, 1995, **77**, 195; P. Huang and A. Petric, *J. Mater. Chem.*, 1995, **5**, 53.

70   E. Ruiz-Trejo and J. A. Kilner, *Solid State Ionics*, 1997, **97**, 33.

71   Y. Larring and T. Norby, *Solid State Ionics*, 1994, **70–71**, 305.

72   K. C. Liang, Y. Du and A. S. Nowick, *Solid State Ionics*, 1994, **69**, 117; A. S. Nowick, Y. Du and K. C. Liang, *Solid State Ionics.*, 1999, **125**, 303; H. G. Bohn, T. Schober, T. Mono and W. Schilling, *Solid State Ionics*, 1999, **117**, 219.

73   M. S. Islam and M. Cherry, *Solid State Ionics*, 1997, **97**, 33; M. Cherry, M. S. Islam, J. D. Gale and C. R. A. Catlow, *J. Phys. Chem.*, 1995, **99**, 14614.

74   R. A. Davies, M. S. Islam and J. D. Gale, *Solid State Ionics*, 1999, **126**, 323; R. Glockner, M. S. Islam and T. Norby, *Solid State Ionics*, 1999, **122**, 145; E. Ruiz-Trejo, M. S. Islam and J. A. Kilner, *Solid State Ionics*, 1999, **123**, 121.

75   K. D. Kreuer, W. Munch, M. Ise, T. He, A. Fuchs, U. Traub and J. Maier, *Ber. Bunsenges. Phys. Chem.*, 1997, **101**, 1344.

76   B. Ammundsen, J. Roziere and M. S. Islam, *J. Phys. Chem. B*,

1997, **101**, 8156; B. Ammundsen, G. R. Burns, M. S. Islam, H. Kanoh and J. Roziere, *J. Phys. Chem. B*, 1999, **103**, 5175.

77 C. Karmonik, T. J. Udovic, R. L. Paul, J. J. Rush, K. Lind and R. Hempelmann, *Solid State Ionics*, 1998, **109**, 207.

78 R. Hempelmann, M. Soetratmo, O. Hartmann and R. Wappling, *Solid State Ionics*, 1998, **107**, 269.

79 W. Munch, G. Seifert, K. D. Kreuer and J. Maier, *Solid State Ionics*, 1996, **86–88**, 647; **97**, 39; F. Shimojo, K. Hoshima and H. Okazaki, *J. Phys.: Condens. Matter*, 1998, **10**, 285.

80 M. S. Islam, R. A. Davies and J. D. Gale, *Chem. Mater.*, 2000, in press.